

# Kolmogorov-Arnold causal generative models

Alejandro Almodóvar  Mar Elizo  Patricia A. Apellániz  Santiago Zazo  Juan Parras 

**Abstract**—Causal generative models provide a principled framework for answering observational, interventional, and counterfactual queries from observational data. However, many deep causal models rely on highly expressive architectures with opaque mechanisms, limiting auditability in high-stakes domains. We propose KaCGM, a causal generative model for mixed-type tabular data where each structural equation is parameterized by a Kolmogorov–Arnold Network (KAN). This decomposition enables direct inspection of learned causal mechanisms, including symbolic approximations and visualization of parent–child relationships, while preserving query-agnostic generative semantics. We introduce a validation pipeline based on distributional matching and independence diagnostics of inferred exogenous variables, allowing assessment using observational data alone. Experiments on synthetic and semi-synthetic benchmarks show competitive performance against state-of-the-art methods. A real-world cardiovascular case study further demonstrates the extraction of simplified structural equations and interpretable causal effects. These results suggest that expressive causal generative modeling and functional transparency can be achieved jointly, supporting trustworthy deployment in tabular decision-making settings.

**Index Terms**—Causal inference, Kolmogorov-Arnold networks, Interpretability, Generative models, Deep learning.

## I. INTRODUCTION

**M**ACHINE learning systems are increasingly deployed in high-stakes domains such as personalized medicine [39, 65], public policy [37], and economics [50], where decisions must be justified, reproducible, and robust to distributional shifts. In these settings, estimating individualized treatment effects and answering counterfactual questions from observational tabular data is central to decision-making. Structural causal models (SCMs) provide a formal framework for such reasoning, allowing the computation of observational, interventional, and counterfactual quantities under explicit assumptions [57, 60]. Recovering a reliable approximation of the underlying SCM is therefore essential for principled policy targeting and individualized care [19].

However, predictive accuracy alone is not sufficient for deployment in sensitive applications. Regulatory frameworks such as the General Data Protection Regulation (GDPR Art. 22) [24], the European Union Artificial Intelligence Act [25], and guidance from the U.S. Food and Drug Administration on AI-enabled medical devices [73] emphasize transparency and accountability requirements for high-risk AI systems. The “right to explanation” and related transparency obligations further reinforce the need for models whose internal logic can be inspected and communicated [31]. In clinical practice, limited interpretability remains a major barrier to the adoption of machine learning systems [6, 72]. As argued by Rudin [63], black-box models are particularly problematic when decisions have substantial real-world consequences and interpretable alternatives are feasible. In the causal setting, interpretability

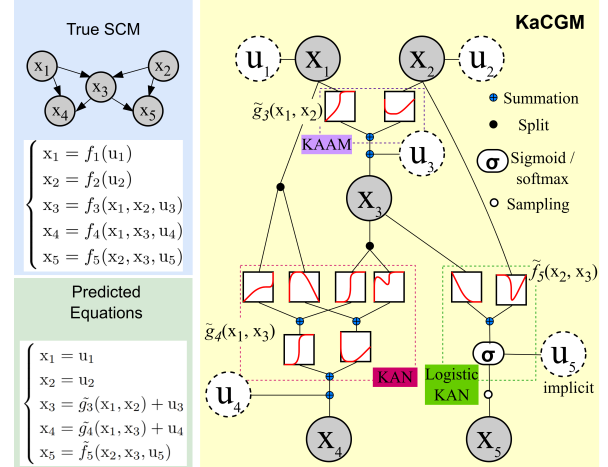


Figure 1: Compacted sketch of the proposed causal generative model, KaCGM, including a discrete variable ( $x_5$ ). The true SCM, with unknown structural equations (left), is approximated with additive noise models in which the functions of each endogenous variable are modeled by KANs (right). Several KANs are shown, in which interpretability capabilities decrease with network complexity. As explained in §IV,  $u_5$  is modeled implicitly by a logistic-KAN. Closed-form expressions can be extracted from every approximated function.

is even more critical: practitioners must understand how interventions propagate through mechanisms, not merely observe predictive correlations.

Recent advances in causal generative models (CGMs) combine deep generative modeling with SCMs, and demonstrate that flexible neural architectures can approximate structural mechanisms while preserving do-operator semantics [17, 38, 55, 66]. These approaches are query-agnostic: once trained, they can answer arbitrary observational, interventional, and counterfactual queries without retraining. Despite these advances, most existing CGMs rely on highly expressive neural networks whose learned structural equations are opaque. While the causal graph itself provides structural interpretability, the functional form of each mechanism remains difficult to audit, simplify, or communicate.

This work addresses the gap between expressive causal generative modeling and functional interpretability in tabular settings. We propose *Kolmogorov-Arnold causal generative model* (KaCGM), a causal generative model in which each structural mechanism is parameterized by a Kolmogorov-Arnold network (KAN). KANs replace scalar weights with learnable univariate functions, inducing structured representations that facilitate inspection, pruning, and symbolic approximation. By embedding KANs within an additive noise SCM framework, our approach preserves generative capabilities and query-agnostic

inference, while supporting the extraction of explicit structural equations.

A compact overview of the proposed model is shown in Fig. 1. Each endogenous variable is modeled as an additive mechanism with exogenous noise, where the structural function is parameterized by a KAN. Mixed data types, including categorical variables, are supported via appropriate likelihood parameterizations. Crucially, closed-form expressions can be extracted from each learned mechanism, enabling direct auditing and visualization of causal effects.

Our contributions are threefold. First, we introduce a KAN-based causal generative model for mixed-type tabular data that preserves SCM semantics and supports observational, interventional, and counterfactual reasoning in a query-agnostic manner. Second, we provide a validation pipeline based on observational distribution matching and independence testing of inferred exogenous noise, enabling practitioners to assess model misspecification from observational data alone. Third, we develop an automated interpretability framework that prunes structural mechanisms, performs symbolic approximation, and extracts closed-form expressions and visualization tools for effect auditing. Code and an interactive interface for visualizing causal effects are publicly available at [github.com/aalmodovares/kacgm](https://github.com/aalmodovares/kacgm) and [huggingface.co/spaces/marElizo/kacgm](https://huggingface.co/spaces/marElizo/kacgm), respectively.

The remainder of this paper is organized as follows. In §II, we review prior work on tabular generative modeling and deep causal generative models. In §III, we recall the formal framework of structural causal models and causal queries. In §IV, we introduce KaCGM, including its additive formulation, mixed-data extension, and interpretability pipeline. In §V, we evaluate the proposed approach on synthetic, semi-synthetic, and real-world datasets, including misspecification analyses and effect visualization. Finally, §VI concludes with a discussion of limitations and future research directions.

## II. RELATED WORK

This work lies at the intersection of generative modeling, causal inference, and interpretable neural architectures. Deep generative models such as generative adversarial networks (GANs) and variational autoencoders (VAEs) have achieved remarkable success in modeling complex data distributions [30, 42]. However, these models typically target the observational joint distribution and lack causal semantics, which limits their ability to answer interventional or counterfactual queries from observational data alone [57].

Causal generative models (CGMs) address this limitation by combining deep generative modeling with the formalism of SCMs, enabling the approximation of data-generating mechanisms while preserving the interventional structure of the SCM [57]. Classical identifiability results for nonlinear additive noise models (ANMs) [36] motivate many recent deep-learning extensions that employ flexible neural architectures to parameterize structural mechanisms and infer exogenous noise variables. Recent approaches span several generative families, including normalizing-flow-based models such as causal flows [38], CAREFL [40], and DCSM [55], as well

as related developments [5, 8, 53, 54]; GAN-based causal generators such as NCM [77] and other frameworks [32, 74, 78]; diffusion-based approaches such as DBCM [17]; and variational models such as VACA [66], among other neural causal modeling approaches [69, 70, 76]. Some of these works further establish theoretical guarantees or identifiability results under additional assumptions, including settings with hidden confounders [5, 53, 54, 77]. While these models provide expressive approximations of SCMs and support query-agnostic inference, the structural mechanisms are typically parameterized by deep neural networks whose functional form is difficult to inspect or audit.

On the other hand, interpretability is a key requirement for deployment in sensitive domains, where models must support auditing, debugging, and transparent decision-making [22]. In tabular prediction tasks, interpretable model families such as generalized additive models and neural additive models have been widely studied [1, 16]. In causal inference, interpretability is further tied to the credibility of estimated effects and the ability to justify “what-if” decisions in terms of mechanisms rather than correlations [57]. Some approaches explore interpretable causal regression through rule-based models [12] or interpretable surrogate models [41]. Nevertheless, although the causal graph provides structural insight, the functional form of the mechanisms learned by causal generative models remains largely opaque.

Recently, Kolmogorov–Arnold networks (KANs) have been proposed as an alternative neural architecture in which scalar weights are replaced by learnable univariate functions defined on edges [47, 48]. This representation induces structured functional decompositions that facilitate inspection, pruning, and symbolic approximation. KANs have rapidly been adapted to multiple architectures, such as convolutional networks [14] or graph neural networks [46], and have demonstrated promising interpretability capabilities in applications such as health-care [3, 58], finance [18], and biology [2]. Their use in causal inference has only recently begun to be explored, for instance, in treatment effect estimation [4, 51].

Building on these developments, this work investigates the use of KANs as structural mechanisms within causal generative models, aiming to combine the flexibility of deep causal generators with interpretable representations of the learned causal mechanisms.

## III. BACKGROUND

### A. Structural Causal Models

Let  $\mathbf{x} = \{x_1, x_2, \dots, x_D\} \in \mathcal{X}$  be a set of random variables with joint distribution  $P_{\mathbf{x}}$ .

**Definition 1.** A causal graph  $\mathcal{G} = (\mathcal{V}, \mathcal{E})$  consists of a set of indices  $\mathcal{V} = \{1, 2, \dots, D\}$  and directed edges  $\mathcal{E}$ , where  $(j, k) \in \mathcal{E}$  denotes that  $x_j$  causally influences  $x_k$ .

Let  $\text{pa}(j)$  denote the set of parents of node  $j$ . If the graph is Markov and faithful [59], the joint distribution factorizes according to the parental Markov condition [57]:

$$p(\mathbf{x}) = \prod_{j=1}^D p(x_j \mid \text{pa}(j)). \quad (1)$$

**Definition 2.** A Structural Causal Model (SCM)  $\mathcal{M} = (\mathbf{f}, P_{\mathbf{u}})$  defines a data-generating process (DGP) where each observed variable is generated from its parents and an exogenous noise variable  $\mathbf{u} = \{u_1, \dots, u_D\}$ :

$$x_j = f_j(\text{pa}(j), u_j), \quad \mathbf{u} \sim P_{\mathbf{u}}. \quad (2)$$

An SCM characterizes the full causal data-generating process and therefore determines the value of any causal query [60]. Interventions are formalized through the do-operator.

**Definition 3** (do-operator [57]). Let  $\mathcal{I} \subseteq \mathcal{V}$ . The intervention  $\text{do}(x_{\mathcal{I}} = a_{\mathcal{I}})$  replaces the structural assignments of the intervened variables by constants, while leaving the remaining mechanisms unchanged.

Causal queries are functionals of the SCM involving at least one intervention, including interventional distributions, causal effects, and counterfactual quantities [57, 60]. SCMs therefore support reasoning at the three levels of Pearl’s hierarchy: observational, interventional, and counterfactual. Interventional distributions are obtained by sampling  $\mathbf{u} \sim P_{\mathbf{u}}$  and propagating the modified structural assignments, while counterfactuals are computed via the abduction–action–prediction procedure [57, 60].

### B. Causal generative models

Causal generative models (CGMs) are generative machine learning models that respect a causal graph  $\mathcal{G}$  and approximate the mechanisms of an SCM  $\mathcal{M}$ . A learned model  $\tilde{\mathcal{M}} = (\tilde{\mathbf{f}}, \tilde{P}_{\mathbf{u}})$  can then be used as a simulator of the underlying causal system.

Once the structural mechanisms are approximated, the model supports observational, interventional, and counterfactual reasoning through the usual do-operator semantics. For continuous variables, under causal sufficiency and with sufficiently expressive function classes, CGMs can recover the structural equations up to standard identifiability considerations [38], leading to consistent answers to causal queries [56, 57].

CGMs are typically *query-agnostic*: once trained, they allow answering arbitrary causal queries without retraining [54]. Recent work has proposed flexible neural CGMs with universal approximation capabilities for SCMs, including models based on normalizing flows, diffusion models, and neural structural mechanisms (see §II). However, most existing approaches rely on highly expressive neural networks whose mechanisms are difficult to interpret.

Although neural networks are universal function approximators, certain classes of functions are known to be more efficiently approximated by spline-based representations, particularly smooth functions in low-data regimes [27]. This motivates exploring alternative architectures that preserve flexibility while improving interpretability, such as Kolmogorov–Arnold networks.

### C. Kolmogorov–Arnold Networks

Kolmogorov–Arnold networks (KANs) provide an alternative representation to deep neural networks. While standard neural networks rely on the universal approximation theorem [35], KANs are inspired by the Kolmogorov–Arnold representation

theorem [7, 44], which states that any continuous function  $f: \mathbb{R}^D \rightarrow \mathbb{R}$  can be expressed as

$$f(\mathbf{x}) = \sum_{k=1}^{2D+1} \Phi_k \left( \sum_{q=1}^D \phi_{k,q}(x_q) \right), \quad (3)$$

where  $\phi$  and  $\Phi$  are univariate nonlinear functions.

Modern implementations approximate these functions using stacked layers, similarly to neural networks [48]. A KAN with  $L$  layers can be written as

$$\text{KAN}(\mathbf{x}) = (\Phi_{L-1} \circ \dots \circ \Phi_0)(\mathbf{x}), \quad (4)$$

where each layer applies sums of learnable univariate functions. In practice, the univariate functions are parameterized with B-splines,

$$\phi(z) = w_b b(z) + w_s \text{spline}(z), \quad (5)$$

with  $b(\cdot)$  a fixed baseline and  $w_s, w_b$  learnable parameters [20]. This formulation allows training with standard optimization methods while maintaining a structured functional representation.

Because KANs explicitly model univariate transformations, they enable direct inspection of nonlinearities and facilitate symbolic approximation and pruning. Additional regularization and sparsification techniques can further simplify the learned functions [47]. In practice, shallow KAN architectures often achieve a favorable balance between expressiveness and interpretability, which has motivated their use in several scientific and applied domains [3, 18, 43].

## IV. KOLMOGOROV-ARNOLD CAUSAL GENERATIVE MODEL

Assume that we have a dataset,  $\mathcal{D} = \{x_1^{(i)}, x_2^{(i)}, \dots, x_D^{(i)}\}_{i=1}^N$ , containing  $N$  i.i.d. samples from the unknown observational distribution  $P_{\mathbf{x}}$ , generated by an unknown SCM  $\mathcal{M}$ , with a known causal graph  $\mathcal{G}$ . Given that, we want to obtain a causal generative model  $\tilde{\mathcal{M}}$  that approximates  $\mathcal{M}$  and, in addition, that provides as many insights about each function  $f_j$  as possible: closed-form equations, interaction terms, symbolic approximations, feature importance, visualization plots of separable effects, etc.

In the following, we assume *causal sufficiency*, i.e., that there are no hidden confounders, and therefore, all the exogenous variables are independent:  $p(\mathbf{u}) = \prod p(u_j)$ .

Our approach, KaCGM, consists of several components. First, we define the KAN-based ANM, which is suitable for continuous variables. Second, we extend it to support discrete or categorical variables. Third, we describe techniques to achieve closed-form equations and plotting tools that help to achieve interpretability.

### A. KaCGM as ANM

KaCGM is an additive noise model (ANM) in which each mechanism of the true SCM is modeled following Eq. 6, where each function that models the effect of the parents on their children,  $\tilde{g}_j(\text{pa}(j))$ , is approximated by a KAN.

$$\tilde{f}_j(\text{pa}(j), u_j) = \tilde{g}_j(\text{pa}(j)) + u_j \quad (6)$$

The choice of ANM has three main motivations: **i**) in the causal inference literature, there are many relevant papers that assume additive noise models to capture real DGPs [15, 36, 52, 67, 68] **ii**) it enables a very interpretable way to understand the exogenous variables as independent additive noise coming from measurement error, a modeling used in fields such as communications [62], robotics [11] or econometrics [28], and **iii**) it is reasonably easy to test if our ANM is a good approximator of the true data-generating process.

Regarding the third point, and although proving that the true DGP is additive is not testable, in general, we can test how well specified our ANM is with respect to the observational data [67]. When facing a real-world problem in which the ground-truth of causal effect cannot be calculated, we recommend testing model misspecification, and only use our model if those tests are satisfactory.

- Test the independence of the exogenous noise:  $u_j \perp\!\!\!\perp \text{pa}(j)$ . Note that we assume that the causal graph is well specified, therefore if the independence condition is not met, it is because of a model misspecification (heteroscedastic noise or nonadditivity), not because the causal direction is reversed [36]. Following Hoyer et al. [36], we propose to use the statistic of the Hilbert-Schmidt Independence test (HSIC) [33]. In the same fashion, we recommend testing that  $\mathbf{u}$  are jointly independent using the multidimensional test dHSIC [61].
- Test the observational match. If a more flexible (e.g. causal flows [38]) model achieves better observational fitting, we consider model misspecification that could mean the DGP is nonadditive. We propose measuring the match of the observational distribution with both *maximum mean discrepancy* (MMD) and classifier two-sample test (C2ST) using the accuracy of a random forest, as explained in §V.

Note that meeting observational matching and independence tests do not allow us to confirm that the true SCM is captured by an ANM, but support well-specification in the sense of “not rejecting misspecification”.

Operation details about training, hyperparameter search, implementation of the do-operator and model misspecification tests can be found in App. B.

### B. Mixed type KaCGM<sub>mix</sub>

In tabular data, there are usually discrete or categorical variables. Therefore, we allow our model to use discrete or categorical models as predictors; in this case, Logistic-KANs. Following the terminology of Almodóvar et al. [3], a Kolmogorov-Arnold additive model (KAAM) is a KAN with no hidden layers, and a Logistic-KAN is a KAN that handles discrete variables by applying a sigmoid function for binary variables or a softmax function for categorical variables. We allow each network within KaCGM<sub>mix</sub> to be a KAAM, a Logistic-KAN, a Logistic-KAAM, or a standard KAN.

We show in Prop. IV.1 how modeling the distribution  $p_\theta(x_j | \text{pa}(j))$  of a categorical variable with a flexible enough

predictor is equivalent to recovering the function  $f_j(\text{pa}(j), u_j)$  with the exogenous term implicit. Although the exogenous term cannot be identified, all interventional queries in the SCM can.

**Proposition IV.1** (mixed CGM equivalence with SCMs). *Consider the true SCM,  $\mathcal{M}$ , in which one variable,  $x_j$  is discrete, with observational probability mass function  $p(x_j | \text{pa}(j))$ . Let  $p_\theta(x_j | \text{pa}(j))$  be a conditional categorical model (e.g. Logistic KAN) such that  $p_\theta(\cdot | \text{pa}(j)) \rightarrow p(\cdot | \text{pa}(j))$ . Being  $F_\theta(\cdot | \text{pa}(j))$  the cumulative density function (CDF) of  $p_\theta$  and defining*

$$\tilde{f}_\theta(\text{pa}(j), u_j) = \min\{k : u \leq F_\theta(k | \text{pa}(j))\}, \quad (7)$$

with  $u_j \sim \mathcal{U}(0, 1)$ . Then **i**)  $x_j = \tilde{f}_\theta(\text{pa}(j), u_j)$  defines a SCM mechanism whose induced conditional law equals  $p_\theta(\cdot | \text{pa}(j))$ : sampling from  $p_\theta(x_j | \text{pa}(j))$  is equivalent to sampling from  $u_j$  and applying  $\tilde{f}_\theta$ ; and **ii**) the interventional distribution of  $x_j$  and its descendants equals the one of  $\mathcal{M}$ .

On the other hand, identifiability of point-valued counterfactuals is not possible with discrete outcomes, and only bounds can be provided [9, 10, 71]. Fortunately, as stated in Prop. IV.2, in a mixed SCM, there exist counterfactual values that can be recovered, depending on the intervention of interest.

**Proposition IV.2** (Counterfactual identifiability in mixed GCM). *Let the partition  $\mathcal{V} = \mathcal{C} \cup \mathcal{Z}$  be the set of indices of the continuous and discrete variables, respectively. Given the intervention on  $\mathcal{I}$ , and let  $\text{de}(\mathcal{I})$  be the descendants of  $\mathcal{I}$  in  $\mathcal{G}$ . Consider a well-specified causal generative model,  $\tilde{\mathcal{M}}$ , in which the map  $u_j \mapsto \tilde{f}_j(\text{pa}(j), u_j)$  for every  $j \in \mathcal{C}$  is injective, then  $\tilde{\mathcal{M}}$  yields point-valued counterfactual predictions if there are not discrete variables in the descendants of  $\mathcal{I}$ , i.e.  $\text{de}(\mathcal{I}) \in \mathcal{C}$ .*

Proofs of Prop. IV.1 and Prop. IV.2 can be found in App. A. Note that both propositions are valid for any CGM that models the distribution of categorical variables.

This adaptation of KaCGM to KaCGM<sub>mix</sub> allows us to increase flexibility when modeling tabular data beyond continuous features, while retaining the identifiability of some causal queries of interest. A sketch of KaCGM<sub>mix</sub> can be observed in Fig. 1, where each function of the true SCM is modeled by a KAN, including the discrete variables, in which the exogenous noise is implicit.

### C. Towards interpretability

Here, we define some steps that highlight the interpretable capabilities of the KANs, including inductive biases towards simplicity that not only regularize the output to get better approximations of smoother functions, but also improve interpretability:

- 1) Between the best KAN models (fail to reject that they are worse than the best), selecting the one with fewer hidden layers (ideally, a KAAM).
- 2) Extract each predicted function  $\tilde{f}_j$ .
- 3) Prune the edges of the KAN that show little importance, following the process described by Liu et al. [47], yielding  $\tilde{f}_j^{(p)}$ . This only removes the non-relevant variables
- 4) Fit a symbolic substitution of  $\tilde{f}_j^{(s)}$  following the process of Almodóvar et al. [4]. This approximates the function

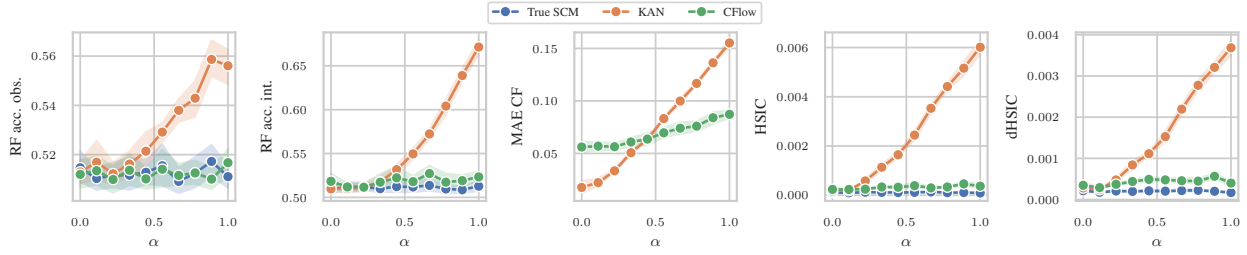


Figure 2: Sensitivity analysis on additivity of exogenous variables. Mean and 95% confidence intervals over 10 realizations of the DGP. The true SCM represents the metrics obtained by data generated by the true SCM. CFlow, as a more flexible model, achieves good approximations and independence even with non-additive noise, while KaCGM deviates from this.

to a combination of atoms: polynomials, trigonometric functions, exponentials, etc.

When performing each of these steps, the well-specification tests described in §IV-A should be carried out. If the results are not satisfactory, the simplification step is **not recommended**. One key observation is that, in each of the steps, the distribution of the residuals should be fitted on observational data again; otherwise, the distribution matching will worsen.

Once we have a satisfactory, simplified  $\hat{f}_j$ , we can either **i)** analyze directly the closed-form expression, which is a composition of univariate functions that could be audited if the number of layers of the selected KAN is low; and **ii)** plot the contribution of each of the parents to the target variable, extracting feature importance, and using the plotting tools developed by Almodóvar et al. [3]: *probability radar plots* (PRP) and *partial dependence plots* (PDP).

Summarizing, the process in a real environment with observational data consists of **i)** constructing and fit KaCGM in observational data, **ii)** testing the observational fit and the independence between exogenous inferred variables, comparing with other more flexible models, **iii)** applying the simplification steps of pruning and symbolic substitution, including tests of step ii), and accept the simplification only if the tests results are not worse up to some threshold established by the user, and **iv)** extracting the closed form expressions of the generating functions and provide interpretable plots.

## V. EXPERIMENTS

We have carried out four experiments to support the use of KaCGM, based on the previous process. This section is organized as follows. First, we present the metrics that we use to measure performance and contrast our hypothesis. Second, we perform a sensitivity analysis where we evaluate how our model suffers from misspecification when the true DGP is not additive, therefore guiding the practitioner through the process in real data. Third, we evaluate the performance of KaCGM in a set of synthetic datasets, of both continuous and discrete data, compared with state-of-the-art CGM, to show that under well specification, the performance of KaCGM is competitive for all data regimes, depending on the amount of data available. Fourth, we present results over a semi-synthetic dataset in which we measure the performance on more complex data. Finally, we implement the previous process in a real-world medical dataset, in which we carry out the misspecification

tests and extract closed expressions of the estimated functions, also providing interpretable plots that help to understand the causal effects in the whole complex system.

### A. Validation metrics

For evaluating the fitting of the observational distribution and the interventional distributions, we use both the maximum mean discrepancy (MMD) [34] with Gaussian kernel and a classifier two samples test (C2ST) [26, 49], where the test accuracy of a random forest (RF) trained with labeled data (real data labeled with 1 and synthetic data labeled with 0) is considered as our test statistic. Less MMD means more similarity between distributions, and an RF accuracy close to chance level (0.5) indicates that the synthetic samples resemble the observational distribution. Second, we use mean absolute error ( $MAE_{CF}$ ) to measure the counterfactual performance.

### B. Sensitivity analysis

We have designed an experiment to test how sensible it is to adopt an additive noise model in a real case. Although in a real dataset we do not have access to the counterfactual error and MMD interventional, we can always measure the fit with the observational distribution and the independence between the extracted exogenous variables. That serves to falsify the additivity of the true DGP.

We generated 6000 samples of the following DGP and used the half for validation.

$$\begin{aligned} x_1 &= u_1 \\ \begin{pmatrix} x_2 \\ x_3 \end{pmatrix} &= \begin{pmatrix} \frac{x_1}{2} + .1x_1^2 + .6u_2 \\ .4x_1 + .1x_1^2 + .7x_2 - \frac{x_2^2}{2} + \frac{x_2^3}{8} - \frac{\alpha x_2 \tanh(u_3 + 1)}{2} + \frac{u_3}{2} \end{pmatrix} \end{aligned}$$

Fig. 2 presents the variation of the metrics used to falsify additivity in the true data-generating process. The charts present how the matching metrics of both observational and interventional distribution vary (MMD obs and MMD int) with  $\alpha$  and how the error in counterfactual estimation varies and how the independence between  $u_3$  and  $pa(3)$  (HSIC) and between  $u_3, u_2, u_1$  (dHSIC) vary with  $\alpha$ . The value of  $\alpha \in [0, 1]$  determines if the DGP is additive ( $\alpha = 0$ ) or not ( $\alpha > 0$ ).

This experiment illustrates how we can reject the use of KaCGM, since a more flexible causal model achieves better observational matching and independence of the residuals when

Model	Continuous variables						Mixed type variables				
	RF <sub>acc</sub> <sup>obs</sup>	MMD <sub>obs</sub> × 10 <sup>-3</sup>	RF <sub>acc</sub> <sup>int</sup>	MMD <sub>int</sub> × 10 <sup>-3</sup>	MAE <sub>CF</sub> × 10 <sup>-2</sup>	p-value	RF <sub>acc</sub> <sup>obs</sup>	MMD <sub>obs</sub> × 10 <sup>-3</sup>	RF <sub>acc</sub> <sup>int</sup>	MMD <sub>int</sub> × 10 <sup>-3</sup>	p-value
KAN	<b>0.51</b> <sub>0.0</sub>	16.49 <sub>8.1</sub>	<b>0.53</b> <sub>0.0</sub>	4.79 <sub>4.1</sub>	5.10 <sub>2.4</sub>	0.061*	<b>0.52</b> <sub>0.02</sub>	1.64 <sub>0.74</sub>	0.54 <sub>0.02</sub>	9.11 <sub>7.24</sub>	0.042
KAAM	0.52 <sub>0.0</sub>	16.76 <sub>9.6</sub>	<b>0.53</b> <sub>0.0</sub>	4.76 <sub>5.1</sub>	4.66 <sub>2.3</sub>	0.055*	<b>0.52</b> <sub>0.01</sub>	1.89 <sub>0.93</sub>	0.54 <sub>0.02</sub>	8.40 <sub>5.63</sub>	0.024
ANM	0.53 <sub>0.0</sub>	<b>8.86</b> <sub>2.6</sub>	0.54 <sub>0.0</sub>	<b>3.02</b> <sub>2.5</sub>	<b>2.62</b> <sub>2.5</sub>	<b>0.500</b> *	0.54 <sub>0.02</sub>	<b>1.22</b> <sub>0.44</sub>	0.56 <sub>0.03</sub>	<b>6.22</b> <sub>5.16</sub>	0.042
DBCM	0.56 <sub>0.0</sub>	31.50 <sub>23.0</sub>	0.55 <sub>0.0</sub>	6.79 <sub>5.8</sub>	3.98 <sub>1.5</sub>	< 1e-3	0.58 <sub>0.04</sub>	3.43 <sub>1.91</sub>	0.57 <sub>0.03</sub>	12.53 <sub>9.90</sub>	< 1e-3
CFlow	0.52 <sub>0.0</sub>	20.46 <sub>6.9</sub>	0.61 <sub>0.1</sub>	9.61 <sub>8.7</sub>	3.86 <sub>1.7</sub>	< 1e-3	0.53 <sub>0.03</sub>	3.16 <sub>1.68</sub>	0.62 <sub>0.09</sub>	7.18 <sub>4.99</sub>	< 1e-3
KAN <sub>mix</sub>	—	—	—	—	—	—	<b>0.52</b> <sub>0.01</sub>	1.79 <sub>0.92</sub>	<b>0.52</b> <sub>0.01</sub>	8.24 <sub>9.88</sub>	<b>0.690</b> *
KAAM <sub>mix</sub>	—	—	—	—	—	—	<b>0.52</b> <sub>0.02</sub>	1.60 <sub>0.78</sub>	<b>0.52</b> <sub>0.01</sub>	6.29 <sub>4.33</sub>	<b>0.690</b> *

Table I: Unified results for continuous and discrete experiments. Metrics report averages over the 11 synthetic datasets (mean<sub>std</sub>) with 1000 training samples. Lower is better for all metrics. Continuous experiments additionally report counterfactual error (MAE<sub>CF</sub>), which is not defined for the discrete setting. The last column of each block reports p-values from post-hoc Wilcoxon tests aggregated over all metrics. The Friedman test p-value is < 1e-3 for both experiments, indicating significant differences among methods overall. Underline denotes the best method. \* indicates no statistically significant difference ( $p > 0.05$ ).

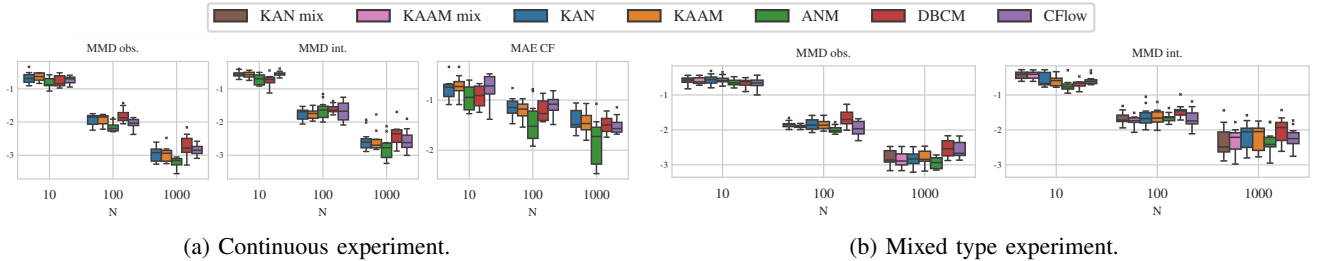


Figure 3: Boxplot of  $\log_{10}$  of observational and interventional MMD of each model across 10 realizations with (a) continuous data and (b) mixed type data, as a function of the number of samples with mixed type data.

the noise is not additive, and this is something that can be tested based on observational data only.

### C. Performance on synthetic datasets

We benchmark our approach to state-of-the-art methods on 11 synthetic graphs obtained from Geffner et al. [29] under different data regimes. We conducted two different experiments, depending on whether all covariates are continuous or if there are discrete variables. All variables are standardized to obtain comparable counterfactual errors across variables. All experiments use the same amount of data for training and testing.

1) *Experiment on continuous data*: We compare the performance of our proposed approaches (KaCGM with KAN and KAAM) to the following methods: DBCM [17] (diffusion-based), causal flows [38] (from now CFlow) and ANM [36] (Additive Noise Model, which selects the best performing method among several classical machine learning tools using regression metrics [13]). Both DBCM and CFlow are universal density approximators, although they need, in principle, larger sample sizes to train [40].

Once the best hyperparameters (details in App. B in supplementary material) are obtained, we proceed to train our final model and validate the results. The validation is done along three main axes: observational, interventional and counterfactual metrics. For *observational metrics*, we compare the RF accuracy and the MMD between the generated distribution and the validation samples. To measure *interventional prediction*, we generate six different interventions over variables  $x_1$  and  $x_2$  (always present in the graph) at standardized values  $x_j = \{-1, 0, 1\}$ . The corresponding interventional distributions

were evaluated using RF accuracy and MMD with the validation samples. Finally, for *counterfactual inference*, we use the validation samples to compute the counterfactual values of each sample using the same interventions defined in the previous point. The counterfactual error is evaluated using MAE (MAE<sub>CF</sub>), compared with the values of the true SCM.

2) *Experiment on mixed data*: For the discrete case, we proceed in a similar fashion, with some key differences. First, we adapt the validation of models designed for continuous variables (CFlow and DBCM) by **i**) adding a small scale noise to the training data (standard deviation 0.01); and **ii**) post-processing the data generated for the discrete variables, by rounding. Second, we add KaCGM<sub>mix</sub> to the evaluation. Third, we discretize one variable,  $x_3 \in \{0, 1, 2\}$ , in the true DGP of Geffner et al. [29] by sampling a ternary variable with probability vectors:  $[0.8, 0.1, 0.1]$  if  $x_3 < -1$ ;  $[0.1, 0.8, 0.1]$  if  $-1 < x_3 < 1$ ; and  $[0.1, 0.1, 0.8]$  if  $x_3 > 1$ . Finally, we do not evaluate counterfactual prediction, since point-valued counterfactuals are not identifiable.

**Results.** The results for 1000 samples can be observed in Tab I, showing close performance of all the models, and the p-values comparing the models in all the metrics together, using the procedure of Demšar [21]. P-values show that **i**) in the continuous case, ANM is the best model, while the two variants of KaCGM are not rejectable as the best models for type I error probability:  $\alpha = 0.05$ , and **ii**) in the discrete case, KaCGM<sub>mix</sub> are the best models across all metrics and realizations, supporting the proposal of using mixed models with discrete data. Note that CFlow and DBCM perform slightly worse because the number of samples is low and the true DGPs of Geffner et al. [29] lie within the ANM class.

Model	Additive						Nonadditive					
	RF <sub>acc</sub> <sup>obs</sup>	MMD <sub>obs</sub> × 10 <sup>-3</sup>	RF <sub>acc</sub> <sup>int</sup>	MMD <sub>int</sub> × 10 <sup>-3</sup>	MAE <sub>CF</sub> × 10 <sup>-2</sup>	p-value	RF <sub>acc</sub> <sup>obs</sup>	MMD <sub>obs</sub> × 10 <sup>-3</sup>	RF <sub>acc</sub> <sup>int</sup>	MMD <sub>int</sub> × 10 <sup>-3</sup>	MAE <sub>CF</sub> × 10 <sup>-2</sup>	p-value
KAN	0.54 <sub>0.02</sub>	1.36 <sub>0.41</sub>	0.54 <sub>0.02</sub>	1.95 <sub>0.67</sub>	3.50 <sub>1.40</sub>	0.180*	0.67 <sub>0.13</sub>	5.27 <sub>9.20</sub>	0.67 <sub>0.14</sub>	6.09 <sub>8.75</sub>	3.42 <sub>1.54</sub>	< 1e-3
KAAM	0.54 <sub>0.01</sub>	1.35 <sub>0.40</sub>	0.55 <sub>0.01</sub>	1.96 <sub>0.74</sub>	3.59 <sub>1.35</sub>	0.180*	0.68 <sub>0.14</sub>	5.97 <sub>9.60</sub>	0.68 <sub>0.14</sub>	6.61 <sub>9.12</sub>	3.56 <sub>1.68</sub>	< 1e-3
ANM	<b>0.53<sub>0.01</sub></b>	<b>1.12<sub>0.28</sub></b>	<b>0.53<sub>0.01</sub></b>	<b>1.30<sub>0.21</sub></b>	<b>1.28<sub>0.43</sub></b>	<b>0.500*</b>	0.61 <sub>0.09</sub>	1.71 <sub>0.83</sub>	0.61 <sub>0.09</sub>	2.31 <sub>1.46</sub>	1.76 <sub>1.13</sub>	0.007
DBCM	0.56 <sub>0.01</sub>	2.78 <sub>0.73</sub>	0.56 <sub>0.01</sub>	2.38 <sub>0.54</sub>	3.03 <sub>0.47</sub>	< 1e-3	0.59 <sub>0.04</sub>	2.61 <sub>0.78</sub>	0.60 <sub>0.04</sub>	2.34 <sub>0.60</sub>	2.67 <sub>0.78</sub>	0.157*
CFlow	0.53 <sub>0.01</sub>	1.42 <sub>0.26</sub>	0.53 <sub>0.01</sub>	1.53 <sub>0.29</sub>	1.69 <sub>0.52</sub>	0.396*	<b>0.55<sub>0.03</sub></b>	<b>1.42<sub>0.35</sub></b>	<b>0.59<sub>0.08</sub></b>	<b>1.84<sub>0.96</sub></b>	<b>1.84<sub>0.99</sub></b>	<b>0.500*</b>

Table II: Results on the Sachs dataset for additive and nonadditive noise settings. Metrics report averages over runs (mean<sub>std</sub>). Lower is better for all metrics. The last column of each block reports p-values from post-hoc Wilcoxon tests aggregated over all metrics. The Friedman test p-value is always < 1e-3, indicating significant differences among methods overall. Underline denotes the best method. \* indicates no statistically significant difference ( $p > 0.05$ ).

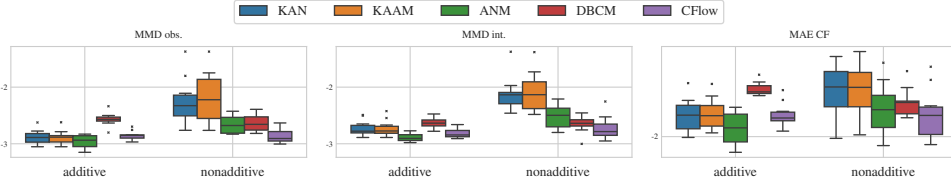


Figure 4: Boxplots of  $\log_{10}$  of observational MMD, interventional MMD and CF MAE on Sachs' semisynthetic dataset. While in the additive setting, all models achieve similar performance, KaCGM worsen significantly in the nonadditive setting.

We also evaluate the impact of the number of samples on the metrics. Hence, for each model and dataset, we compute all metrics using 1000, 100 and 10 training (and test) samples. When the number of samples decreases, the metrics worsen, as expected: this behavior can be observed in Fig. 3.

#### D. Performance in semi-synthetic dataset

Following other works [5, 17], we also validate our approach on a more complex semi-synthetic dataset, created following the process procedure by Chao et al. [17], from the original dataset of Sachs et al. [64]. The dataset contains 11 variables associated with the causal graph of Fig. 6. Root nodes are sampled from the original dataset, while the other variables are generated using random equations.

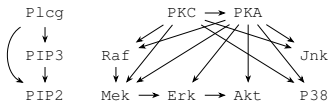


Figure 6: Causal graph associated with Sachs' dataset.

We generate 1000 training samples and also 1000 validation samples in both additive and nonadditive settings. The results using the same evaluation method from the previous experiment can be seen in Tab II. In the additive setting, ANM achieves the best results in all metrics, while KaCGM and CFlows (in particular causal masked autoregressive flows, CausalMAF, which is also an additive model) get comparable results, while DBCM is not competitive with this number of samples. On the other hand, in the nonadditive settings, causal flows (in particular, causal neural spline flows, CausalNSF, which is more flexible) achieves the best results, with DBCM presenting a competitive performance. These findings can also be observed in Fig. 4.

#### E. Use case: cardiovascular data

We illustrate the interpretability capabilities of our approach on a real-world cardiovascular dataset whose goal is to estimate the probability of a *major acute cardiovascular event* (MAC). The dataset, introduced by Kyriacou et al. [45], contains continuous and binary clinical covariates together with a causal graph that we assume to be correct and is shown in Fig. 7.

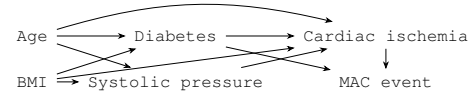


Figure 7: Causal graph of cardio dataset. The original graph contained *obesity* and *hypertension*; we instead use their continuous counterparts BMI and systolic pressure.

Since true interventional distributions or counterfactual outcomes are not available, the evaluation must rely on observational diagnostics. Following the validation pipeline described in §IV, we train KaCGM<sub>mix</sub> using KAN and KAAM subnetworks and compare it with the baselines. In addition, we apply the simplification pipeline (pruning and symbolic substitution) and evaluate how these transformations affect the observational fit.

The results are summarized in Fig. 5. Pruning preserves the observational performance, whereas symbolic substitution slightly degrades the metrics, illustrating the expected trade-off between predictive fidelity and interpretability. Nevertheless, KaCGM<sub>mix</sub> achieves competitive observational fit, obtaining the best RF accuracy and MMD among the compared models, although independence diagnostics are less favorable. This analysis supports the use of the simplified models when interpretability is a primary objective.

The key advantage of the proposed model is that the structural mechanisms can be explicitly inspected. For example, after pruning and symbolic approximation, the probability of

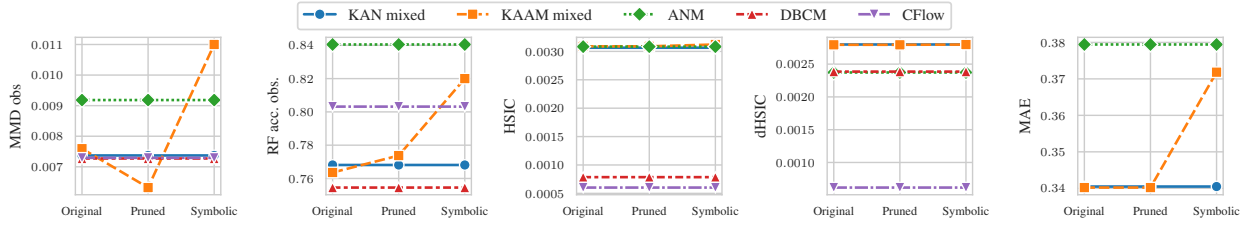


Figure 5: Observational metrics on the cardiovascular dataset as a function of the simplification stage. MAE denotes predictive error when estimating each node from its parents. DBCM and CFlow cannot compute conditional samples and, therefore, MAE is not reported. HSIC and dHSIC are evaluated only for continuous variables.

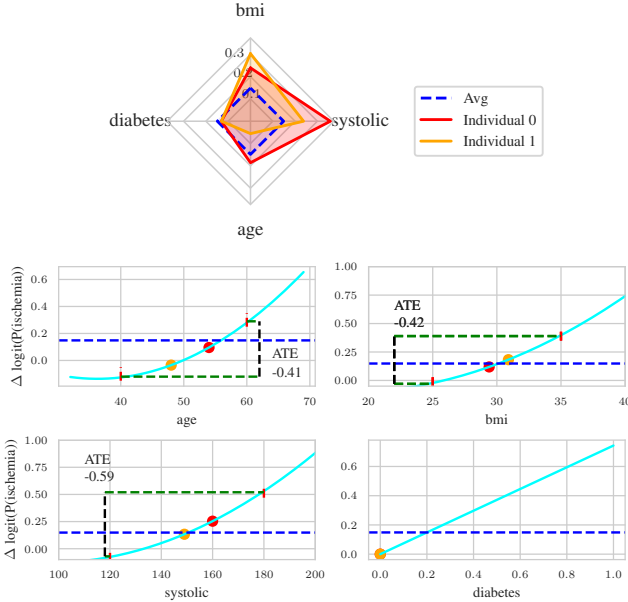


Figure 8: Interpretability analysis of the ischemia mechanism. (Top) PRPs showing the contribution of each parent variable to the logit for two individuals. (Bottom) PDPs representing the contribution  $\Delta$  of each variable to the logit. The curves also allow direct computation of average treatment effects (ATE) corresponding to hypothetical interventions on each variable.

cardiac ischemia conditioned on its parents can be expressed as

$$\begin{aligned} \Pr(\text{ischemia}) = & \sigma(0.055 \overline{\text{age}}^2 + 0.173 \overline{\text{age}} \\ & + 0.031 \overline{\text{BMI}}^2 + 0.114 \overline{\text{BMI}} \\ & + 0.046 \overline{\text{systolic}}^2 + 0.155 \overline{\text{systolic}} \\ & + 0.743 \overline{\text{diabetes}} - 1.871), \end{aligned}$$

where  $\sigma$  represents the sigmoid function and the overline variables are standardized. This expression provides a transparent representation of the learned causal mechanism that can be directly audited by domain experts. For instance, the logit of the ischemia probability increases quadratically with both age and systolic pressure, a pattern that is consistent with clinical intuition: cardiovascular risk is known to grow nonlinearly with aging and with elevated blood pressure. Similarly, BMI contributes through both linear and quadratic terms, capturing

increasing risk at higher levels of body mass.

Beyond the closed-form expression, the interpretability tools allow for visualizing how each variable contributes to the predicted outcome. Fig. 8 illustrates this through two complementary visualizations. The probability radar plots (PRP) decompose the contribution of each parent variable to the logit for two randomly selected individuals. In the example shown, Individual 0 exhibits higher ischemia risk due to greater age and systolic pressure, whereas Individual 1 has elevated BMI, which also increases the predicted probability.

The probability dependence plots (PDPs) provide a complementary population-level view of the learned mechanisms. These plots display how each parent variable contributes to the logit of the ischemia probability while marginalizing over the remaining variables. Because the structural equation is explicit, these curves also allow straightforward estimation of average treatment effects (ATE) corresponding to hypothetical interventions on each variable.

For instance, the PDPs in Fig. 8 show how changes in BMI and systolic pressure modify the logit of the ischemia probability. From these curves, the ATE of reducing BMI from 35 to 20 is approximately  $-0.42$  in the logit scale, while lowering systolic pressure from 180 to 120 yields an ATE of approximately  $-0.59$ . These quantities correspond to population-level intervention effects estimated directly from the learned structural equation.

Importantly, these effects are not obtained from a black-box predictor but from an explicit functional representation of the mechanism. Consequently, practitioners can both visualize the nonlinear contribution of each variable and compute interpretable causal summaries such as ATEs directly from the model.

We provide the code of all the experiments for reproducibility in [github.com/aalmodovares/kacgm](https://github.com/aalmodovares/kacgm). We also include an online interactive interface, in which the causal effects of every variable in the Sachs' dataset and in the usecase can be explored and audited, in [huggingface.co/spaces/marElizo/kacgm](https://huggingface.co/spaces/marElizo/kacgm).

## VI. CONCLUDING REMARKS

This work investigated the integration of Kolmogorov-Arnold networks within causal generative modeling for tabular data. We proposed KaCGM, a causal generative model that preserves the semantics of structural causal models while enabling direct inspection of the learned structural mechanisms. KaCGM is

a query-agnostic model capable of answering observational, interventional, and counterfactual queries, while supporting symbolic simplification, pruning, and functional visualization.

Empirically, the results presented in §V demonstrate that, under additive data-generating processes, KaCGM achieves performance comparable to optimal additive noise models and competitive with state-of-the-art deep causal generative models in terms of observational fit, interventional distribution matching, and counterfactual accuracy. In mixed continuous–discrete settings, the proposed extension maintains competitive performance while preserving interpretability of the structural equations. The sensitivity analysis further illustrates that model misspecification can be detected using independence tests on inferred exogenous variables and distributional metrics, providing practical guidance for deployment under observational data alone. In semi-synthetic experiments, KaCGM performs strongly when the additive assumption is satisfied, while more flexible deep causal models outperform it in strongly nonadditive regimes. This trade-off highlights the central design principle of our approach: favoring structural interpretability and auditability when the data-generating process is compatible with additive mechanisms. Finally, in the real-world cardiovascular use case, we demonstrated that the model can achieve competitive observational performance while enabling the extraction of simplified structural equations and interpretable visualizations of causal effects. These results support the feasibility of combining expressive generative modeling with functional transparency, a property that is particularly relevant for high-stakes applications where auditing and mechanistic understanding are required.

Despite its advantages, the proposed approach presents several limitations. First, the model relies on structural mechanisms that admit relatively low-complexity functional decompositions. When the true data-generating process exhibits strongly nonadditive, highly entangled, or heteroscedastic interactions, more flexible deep causal generative models can achieve superior density approximation and counterfactual accuracy, as observed in §V. In such regimes, enforcing structured functional representations may lead to approximation bias. Second, interpretability is inherently tied to model simplification. Pruning and symbolic approximation improve transparency but may degrade predictive fidelity, introducing a trade-off between auditability and accuracy. While our validation pipeline mitigates this risk through independence and distributional diagnostics, it cannot guarantee that the learned mechanisms coincide with the true structural equations, particularly under model misspecification. Third, the methodology assumes causal sufficiency and a correctly specified causal graph. Violations of these assumptions, such as hidden confounding or graph misspecification, can invalidate the generative interpretation and the associated counterfactual estimates. Finally, although the approach scales to moderate-dimensional tabular settings, extracting symbolic expressions and visual diagnostics becomes increasingly challenging as graph size and mechanism complexity grow. Addressing these limitations requires balancing interpretability, expressivity, and scalability in future work.

Several directions for future research arise from this work. First, one may extend the architecture to increase density

approximation flexibility while preserving interpretability. In particular, KAN-based normalizing flow constructions could allow more expressive transformations of the exogenous variables, including neural spline flows [23] or unconstrained monotonic neural networks [75]. Such extensions would require new interpretability tools to ensure that increased flexibility does not compromise auditability. Second, alternative functional bases beyond spline parameterizations may be explored, such as Fourier expansions [46], which could provide improved inductive biases in periodic or oscillatory mechanisms. Third, assessing partial well-specification represents an important practical direction. Instead of requiring global model adequacy, one may restrict attention to subsets of intervention targets for which additive structure is sufficiently accurate, as suggested in recent work on partial model validation [67]. Another promising avenue is regression by dependence minimization [52], enforcing independence between inferred exogenous variables and their parents to strengthen structural validity.

Finally, extending the methodology beyond causal sufficiency remains an open challenge. Incorporating proxy-based adjustments [5] or leveraging graph transformations that yield equivalent identifiable structures [54] would broaden applicability to settings with hidden confounding.

In summary, this work advances interpretable causal generative modeling by demonstrating that structured, additive neural architectures can provide competitive performance while enabling direct inspection of structural equations. We hope this contribution encourages further research at the intersection of causal modeling, generative learning, and functional interpretability.

#### Bibliography:

- [1] Agarwal, R., Melnick, L., Frosst, N., Zhang, X., Lengerich, B., Caruana, R., and Hinton, G.E. Neural additive models: Interpretable machine learning with neural nets, 2021. [↗](#)
- [2] Alharbi, F., Budhiraja, N., Vakanski, A., Zhang, B., Elbashir, M., Guduru, H., and Mohammed, M. Interpretable graph kolmogorov–arnold networks for multi-cancer classification and biomarker identification using multi-omics data. *Scientific Reports*, 15, 07 2025. doi: 10.1038/s41598-025-13337-0
- [3] Almodóvar, A., Apellániz, P.A., Garrido, A., Fernández-Salvador, F., Zazo, S., and Parras, J. Interpretable clinical classification with Kolmogorov-Arnold Networks. *arXiv preprint arXiv:2509.16750*, 2025
- [4] Almodóvar, A., Apellániz, P.A., Zazo, S., and Parras, J. CausalKANs: interpretable treatment effect estimation with Kolmogorov-Arnold networks. *arXiv preprint arXiv:2509.22467*, 2025
- [5] Almodóvar, A., Javaloy, A., Parras, J., Zazo, S., and Valera, I. DeCaFlow: A deconfounding causal generative model. In *The Thirty-ninth Annual Conference on Neural Information Processing Systems*, 2025. doi: 10.48550/arXiv.2503.15114. [↗](#)
- [6] Amann, J., Blasimme, A., Vayena, E., Frey, D., and Madai, V.I. Explainability for artificial intelligence in healthcare: a multidisciplinary perspective. *BMC Medical Informatics*

- and Decision Making, 20(310), 2020. doi: 10.1186/s12911-020-01332-6
- [7] Arnold, V.I. On functions of three variables. *Doklady Akademii Nauk SSSR*, 114:679–681, 1957. English translation in *American Mathematical Society Translations*, Series 2, Vol. 28: Sixteen Papers on Analysis, 1963, pp. 51–54
- [8] Balgi, S., Daoud, A., Pena, J.M., Wodtke, G.T., and Zhou, J. Deep learning with dags. *Sociological Methods & Research*, page 00491241251319291, 2025
- [9] Balke, A. and Pearl, J. Probabilistic evaluation of counterfactual queries. In *Proceedings of the Twelfth National Conference on Artificial Intelligence (AAAI-94)*. AAAI press, 1994
- [10] Balke, A. and Pearl, J. Bounds on treatment effects from studies with imperfect compliance. *Journal of the American statistical Association*, 92(439):1171–1176, 1997
- [11] Barfoot, T.D. *State estimation for robotics*. Cambridge University Press, 2024
- [12] Bargagli-Stoffi, F.J., Cadei, R., Lee, K., and Dominici, F. Causal rule ensemble: Interpretable discovery and inference of heterogeneous treatment effects. *arXiv preprint arXiv:2009.09036*, 2020
- [13] Blöbaum, P., Götz, P., Budhathoki, K., Mastakouri, A.A., and Janzing, D. Dowhy-gcm: An extension of dowhy for causal inference in graphical causal models. *Journal of Machine Learning Research*, 25(147):1–7, 2024. [↗](#)
- [14] Bodner, A.D., Spolski, J.N., Tepsich, A.S., and Pourteau, S. Convolutional kolmogorov-arnold networks, 2025. [↗](#)
- [15] Bühlmann, P., Peters, J., and Ernest, J. Cam: Causal additive models, high-dimensional order search and penalized regression. *The Annals of Statistics*, 42(6), 2014
- [16] Caruana, R., Lou, Y., Gehrke, J., Koch, P., Sturm, M., and Elhadad, N. Intelligible models for healthcare: Predicting pneumonia risk and hospital 30-day readmission. In *Proceedings of the 21th ACM SIGKDD international conference on knowledge discovery and data mining*, pages 1721–1730, 2015
- [17] Chao, P., Blöbaum, P., Patel, S., and Kasiviswanathan, S.P. Modeling causal mechanisms with diffusion models for interventional and counterfactual queries. *Transactions on Machine Learning Research*, 2024. [↗](#)
- [18] Cho, S.Y., Lee, S., and Kim, H.G. Forecasting vix using interpretable kolmogorov-arnold networks. *Expert Systems with Applications*, 294:128781, 2025. ISSN 0957-4174. doi: <https://doi.org/10.1016/j.eswa.2025.128781>
- [19] Curth, A., Peck, R.W., McKinney, E., Weatherall, J., and van der Schaar, M. Using machine learning to individualize treatment effect estimation: Challenges and opportunities. *Clinical Pharmacology & Therapeutics*, 115(4):710–719, 2024. doi: 10.1002/cpt.3159
- [20] De Boor, C. and De Boor, C. *A practical guide to splines*, volume 27. springer New York, 1978
- [21] Demšar, J. Statistical comparisons of classifiers over multiple data sets. *Journal of Machine learning research*, 7(Jan):1–30, 2006
- [22] Doshi-Velez, F. and Kim, B. Towards a rigorous science of interpretable machine learning, 2017. [↗](#)
- [23] Durkan, C., Bekasov, A., Murray, I., and Papamakarios, G. Neural spline flows. *Advances in neural information processing systems*, 32, 2019
- [24] European Parliament and Council, . Regulation (EU) 2016/679 (GDPR) on the protection of natural persons with regard to the processing of personal data and on the free movement of such data. Official Journal of the European Union, 2016
- [25] European Parliament and Council, . Regulation (EU) 2024/1689 (Artificial Intelligence Act). Official Journal of the European Union, 2024. Transparency and information requirements for high-risk AI systems
- [26] Friedman, J. On multivariate goodness-of-fit and two-sample testing. Technical report, Stanford Linear Accelerator Center, Menlo Park, CA (US), 01 2004. [↗](#)
- [27] Friedman, J. Adaptive spline networks. In Lippmann, R., Moody, J., and Touretzky, D., editors, *Advances in Neural Information Processing Systems*, volume 3. Morgan-Kaufmann, 1990. [↗](#)
- [28] Fuller, W.A. *Measurement error models*. John Wiley & Sons, 2009
- [29] Geffner, T., Antoran, J., Foster, A., Gong, W., Ma, C., Kiciman, E., Sharma, A., Lamb, A., Kukla, M., Pawlowski, N., and others, . Deep end-to-end causal inference. *arXiv preprint arXiv:2202.02195*, 2022
- [30] Goodfellow, I., Pouget-Abadie, J., Mirza, M., Xu, B., Warde-Farley, D., Ozair, S., Courville, A., and Bengio, Y. Generative adversarial networks. *Communications of the ACM*, 63(11):139–144, 2020
- [31] Goodman, B. and Flaxman, S. European union regulations on algorithmic decision-making and a “right to explanation”. *AI magazine*, 38(3):50–57, 2017
- [32] Goudet, O., Kalainathan, D., Caillou, P., Guyon, I., Lopez-Paz, D., and Sebag, M. *Learning Functional Causal Models with Generative Neural Networks*, pages 39–80. Springer International Publishing, Cham, 2018. doi: 10.1007/978-3-319-98131-4\_3. [↗](#)
- [33] Gretton, A., Bousquet, O., Smola, A., and Schölkopf, B. Measuring statistical dependence with hilbert-schmidt norms. In *International conference on algorithmic learning theory*, pages 63–77. Springer, 2005
- [34] Gretton, A., Borgwardt, K.M., Rasch, M.J., Schölkopf, B., and Smola, A. A kernel two-sample test. *The journal of machine learning research*, 13(1):723–773, 2012
- [35] Hornik, K., Stinchcombe, M., and White, H. Multilayer feedforward networks are universal approximators. *Neural networks*, 2(5):359–366, 1989
- [36] Hoyer, P.O., Janzing, D., Mooij, J.M., Peters, J., and Schölkopf, B. Nonlinear causal discovery with additive noise models. In *Advances in Neural Information Processing Systems 21 (NeurIPS 2008)*, pages 689–696, 2009. [↗](#)
- [37] Imai, K. and Strauss, A. Estimation of heterogeneous treatment effects from randomized experiments, with application to the optimal planning of the get-out-the-vote campaign. *Political Analysis*, 19(1):1–19, 2011. doi:

- 10.1093/pan/mpq035
- [38] Javaloy, A., Sánchez-Martín, P., and Valera, I. Causal normalizing flows: from theory to practice. *Advances in Neural Information Processing Systems*, 36:58833–58864, 2023
- [39] Kent, D.M., Steyerberg, E., and van Klaveren, D. Personalized evidence based medicine: predictive approaches to heterogeneous treatment effects. *BMJ*, 363:k4245, 2018. doi: 10.1136/bmj.k4245
- [40] Khemakhem, I., Monti, R.P., Leech, R., and Hyvärinen, A. Causal autoregressive flows. In *Proceedings of the 24th International Conference on Artificial Intelligence and Statistics (AISTATS 2021)*, 2021. [↗](#)
- [41] Kim, C. and Bastani, O. Learning interpretable models with causal guarantees. *arXiv preprint arXiv:1901.08576*, 2019
- [42] Kingma, D.P. and Welling, M. Auto-encoding variational bayes. *arXiv preprint arXiv:1312.6114*, 2013
- [43] Knottenbelt, W., McGough, W., Wray, R., Zhang, W.Z., Liu, J., Machado, I.P., Gao, Z., and Crispin-Ortuzar, M. Coxkan: Kolmogorov-arnold networks for interpretable, high-performance survival analysis. *Bioinformatics*, 41(8):btaf413, 07 2025. ISSN 1367-4811. doi: 10.1093/bioinformatics/btaf413. [↗](#)
- [44] Kolmogorov, A.N. On the representations of continuous functions of many variables by superposition of continuous functions of one variable and addition. In *Dokl. Akad. Nauk USSR*, volume 114, pages 953–956, 1957
- [45] Kyriacou, D.N., Greenland, P., and Mansournia, M.A. Using causal diagrams for biomedical research. *Annals of Emergency Medicine*, 81(5):606–613, 2023. ISSN 0196-0644. doi: <https://doi.org/10.1016/j.annemergmed.2022.08.014>. [↗](#)
- [46] Li, L., Zhang, Y., Wang, G., and Xia, K. Kolmogorov-arnold graph neural networks for molecular property prediction. *Nature Machine Intelligence*, 7(8):1346–1354, 2025
- [47] Liu, Z., Ma, P., Wang, Y., Matusik, W., and Tegmark, M. Kan 2.0: Kolmogorov-arnold networks meet science. *arXiv preprint arXiv:2408.10205*, 2024
- [48] Liu, Z., Wang, Y., Vaidya, S., Ruehle, F., Halverson, J., Soljačić, M., Hou, T.Y., and Tegmark, M. KAN: Kolmogorov-arnold networks. In *The Thirteenth International Conference on Learning Representations (ICLR 2025)*, 2025. [↗](#)
- [49] Lopez-Paz, D. and Oquab, M. Revisiting classifier two-sample tests. In *International Conference on Learning Representations*, 2017. [↗](#)
- [50] Manski, C.F. Statistical treatment rules for heterogeneous populations. *Econometrica*, 72(4):1221–1246, 2004
- [51] Mehendale, E., Thorat, A., Kolla, R., and Pedaneekar, N. Kanite: Kolmogorov-arnold networks for ite estimation. In *Joint European Conference on Machine Learning and Knowledge Discovery in Databases*, pages 409–425. Springer, 2025
- [52] Mooij, J., Janzing, D., Peters, J., and Schölkopf, B. Regression by dependence minimization and its application to causal inference in additive noise models. In *Proceedings of the 26th annual international conference on machine learning*, pages 745–752, 2009
- [53] Nasr-Esfahany, A., Alizadeh, M., and Shah, D. Counterfactual identifiability of bijective causal models. In *International Conference on Machine Learning*, pages 25733–25754. PMLR, 2023
- [54] Parafita, Á. and Vitría, J. Estimand-agnostic causal query estimation with deep causal graphs. *IEEE Access*, 10: 71370–71386, 2022
- [55] Pawlowski, N., Castro, D.C., and Glocker, B. Deep structural causal models for tractable counterfactual inference. In *Advances in Neural Information Processing Systems 33 (NeurIPS 2020)*, 2020. [↗](#)
- [56] Pearl, J. Probabilities of causation: Three counterfactual interpretations and their identification. *Synthese*, 121(1): 93–149, 1999
- [57] Pearl, J. *Causality: Models, Reasoning, and Inference*. Cambridge University Press, 2 edition, 2009
- [58] Pendyala, V.S. and Venkatachalam, N. The effectiveness of kolmogorov-arnold networks in the healthcare domain. *Applied Sciences*, 15(16), 2025. ISSN 2076-3417
- [59] Peters, J., Janzing, D., and Schölkopf, B. Causal inference on discrete data using additive noise models. *IEEE Transactions on Pattern Analysis and Machine Intelligence*, 33(12):2436–2450, 2011
- [60] Peters, J., Janzing, D., and Schölkopf, B. *Elements of causal inference: foundations and learning algorithms*. The MIT press, 2017
- [61] Pfister, N., Bühlmann, P., Schölkopf, B., and Peters, J. Kernel-based tests for joint independence. *Journal of the Royal Statistical Society Series B: Statistical Methodology*, 80(1):5–31, 2018
- [62] Proakis, J.G., Salehi, M., Zhou, N., and Li, X. *Communication systems engineering*, volume 2. Prentice Hall New Jersey, 1994
- [63] Rudin, C. Stop explaining black box machine learning models for high stakes decisions and use interpretable models instead. *Nature machine intelligence*, 1(5):206–215, 2019
- [64] Sachs, K., Perez, O., Pe’er, D., Lauffenburger, D.A., and Nolan, G.P. Causal protein-signaling networks derived from multiparameter single-cell data. *Science*, 308(5721): 523–529, 2005
- [65] Sanchez, P., Voisey, J.P., Xia, T., Watson, H.I., O’Neil, A.Q., and Tsaftaris, S.A. Causal machine learning for healthcare and precision medicine. *Royal Society Open Science*, 9(8):220638, 2022
- [66] Sánchez-Martín, P., Rateike, M., and Valera, I. Vaca: Designing variational graph autoencoders for causal queries. In *Proceedings of the AAAI Conference on Artificial Intelligence*, volume 36, pages 8159–8168, 2022
- [67] Schultheiss, C. and Bühlmann, P. Assessing the overall and partial causal well-specification of nonlinear additive noise models. *Journal of Machine Learning Research*, 25(159):1–41, 2024. [↗](#)
- [68] Shimizu, S., Hoyer, P.O., Hyvärinen, A., Kerminen, A., and Jordan, M. A linear non-gaussian acyclic model for causal discovery. *Journal of Machine Learning Research*,

7(10), 2006

- [69] Sick, B. and Dürr, O. Interpretable neural causal models with tram-dags. *arXiv preprint arXiv:2503.16206*, 2025
- [70] Stegle, O., Janzing, D., Zhang, K., Mooij, J.M., and Schölkopf, B. Probabilistic latent variable models for distinguishing between cause and effect. *Advances in neural information processing systems*, 23, 2010
- [71] Tian, J. and Pearl, J. Probabilities of causation: Bounds and identification. *Annals of Mathematics and Artificial Intelligence*, 28(1):287–313, 2000
- [72] Tonekaboni, S., Joshi, S., McCradden, M.D., and Goldenberg, A. What clinicians want: Contextualizing explainable machine learning for clinical end use. In *Proceedings of the 4th Machine Learning for Healthcare Conference*, volume 106, pages 359–380. PMLR, 2019
- [73] U.S. Food and Drug Administration, Health Canada, MHRA, . Transparency for machine learning-enabled medical devices: Guiding principles, 2024. [↗](#)
- [74] Van Breugel, B., Kyono, T., Berrevoets, J., and Van der Schaar, M. DECAF: Generating fair synthetic data using causally-aware generative networks. *Advances in Neural Information Processing Systems*, 34:22221–22233, 2021
- [75] Wehenkel, A. and Louppe, G. Unconstrained monotonic neural networks. *Advances in neural information processing systems*, 32, 2019
- [76] Xia, K., Lee, K.Z., Bengio, Y., and Bareinboim, E. The causal-neural connection: Expressiveness, learnability, and inference. *Advances in Neural Information Processing Systems*, 34:10823–10836, 2021
- [77] Xia, K.M., Pan, Y., and Bareinboim, E. Neural causal models for counterfactual identification and estimation. In *The Eleventh International Conference on Learning Representations*, 2023
- [78] Xu, D., Wu, Y., Yuan, S., Zhang, L., and Wu, X. Achieving causal fairness through generative adversarial networks. In *Proceedings of the Twenty-Eighth International Joint Conference on Artificial Intelligence*, 2019

## APPENDIX

### A. Proofs

*Proof of Prop. IV.1. ii* Intervening in  $x_q \in \text{pa}(j)$ ,  $\text{do}(x_q = \alpha)$ , the mechanism is  $x = \tilde{f}_\theta(\alpha, \text{pa}(j)_{-q}, u_j)$ . Conditioning on  $\text{pa}(j)_{-q}$ , and having that  $u_j \perp\!\!\!\perp \text{pa}(j)$ :

$$\begin{aligned} p_\theta(x_j \mid \text{do}(x_q = \alpha), \text{pa}(j)) &= P(\tilde{f}_\theta(\alpha, \text{pa}(j), u_j) = x_j) \\ &= p_\theta(x \mid \alpha, \text{pa}(j)). \end{aligned}$$

For descendants of  $x_j$ , with downstream mechanisms fixed, the interventional law factorizes as a mixture over  $x_j$  with weights  $p_\theta(x_j \mid \text{do}(\alpha), \text{pa}(j)_{-q})$ . Convergence in these weights implies convergence in distribution of the induced descendants.  $\square$

*Proof of Prop. IV.2.* Since  $\text{de}(\mathcal{I}) \in \mathcal{C}$  For each variable  $j \in \text{de}(\mathcal{I})$ , every parent of  $j$  lies **i** in  $\mathcal{I}$ , **ii** in  $\text{de}(\mathcal{I})$  or **iii** outside  $\text{de}(\mathcal{I})$ . In the abduction-action-prediction process, given a factual point,  $x^f$ , **i** is fixed by intervention, **ii** is computed

earlier in the topological evaluation and **iii** keep their factual values. Thus, the inputs to  $\tilde{f}_j$  are uniquely determined (in addition to  $\tilde{u}_j = \tilde{f}_j^{-1}(\text{pa}(j), x_j^f)$ ), which gives a unique value of the counterfactual  $x_{j,\text{do}(x_T)}^{\text{cf}}$ .  $\square$

### B. Operation of KaCGM

Details of training (Alg. 1), the do-operator implementation (Alg. 4 and Alg. 5) and assumptions falsification (Alg. 3). Without loss of generality, assume that  $\mathbf{x}$  are in causal order.  $\mathcal{R}$  is the regularization term of KANs.

---

#### Algorithm 1 Training

---

**Require:** Dataset  $\mathcal{D}$   
**Ensure:**  $\{\theta_j^*\}_{j=1}^D, \{\tilde{p}(u_j)\}_{j=1}^D$   
1: **for**  $j = 1$  to  $D$  **do**  
2:    $\lambda_j^* = \arg \min_\lambda [\min_{\theta} \mathcal{L}]$   
3:    $\theta_j^* = \arg \min_{\theta \in \Theta(\lambda_j^*)} \text{MSE}(x_j, \text{KAN}_{\theta}^{(j)}(\text{pa}(x_j))) + \mathcal{R}$   
4:    $\tilde{u}_j \leftarrow \text{ObtainResiduals}(\mathcal{D}, f_{\theta^*}) // \text{Alg. 2}$   
5:    $\tilde{p}(u_j) \leftarrow \text{EstimateDistribution}(\tilde{u}_j)$   
6: **end for**  
7: **return**  $\{\theta_j^*\}_{j=1}^D, \{\tilde{p}(u_j)\}_{j=1}^D$

---



---

#### Algorithm 2 Obtain Residuals

---

**Require:** Dataset  $\mathcal{D}$ , functions  $f_\theta = \{\tilde{f}\}_{j=1}^D$   
**Ensure:**  $\{\{\tilde{u}_j^{(i)}\}_{i=1}^N\}_{j=1}^D$   
1: **for**  $i = 1$  to  $N$  **do**  
2:   **for**  $j = D$  down to  $1$  **do**  
3:      $\tilde{u}_j^{(i)} \leftarrow x_j^{(i)} - \tilde{f}(\text{pa}(j)^{(i)})$   
4:   **end for**  
5: **end for**  
6: **return**  $\{\{\tilde{u}_j^{(i)}\}_{j,i}\}$

---



---

#### Algorithm 3 Falsify Assumptions

---

**Require:** Dataset  $\mathcal{D}$ , functions  $f_\theta$ , intervention set  $\mathcal{I}$   
**Ensure:**  $\{\text{p-value}_j\}_{j=1}^D$ , MMD,  $\text{RF}_{\text{acc}}$   
1:  $\{\{\tilde{u}_j^{(i)}\}\} \leftarrow \text{ObtainResiduals}(\mathcal{D}, f_\theta) // \text{Alg. 2}$   
2: **for**  $j = 1$  to  $D$  **do**  
3:    $\text{stat}_j \leftarrow \text{HSIC}(\{\tilde{u}_j^{(i)}\}_{i=1}^N, \{\text{pa}(j)^{(i)}\}_{i=1}^N)$   
4: **end for**  
5: **for**  $j \in \{1, \dots, D\} \setminus \mathcal{I}$  **do**  
6:   Sample  $\{u_j^{(k)}\}_{k=1}^M \sim \tilde{p}(u_j)$   
7:    $x_j^{(k)} \leftarrow \tilde{f}(\text{pa}(j)^{(k)}) + u_j^{(k)}$   
8: **end for**  
9:  $\text{MMD} \leftarrow \text{MMD}(\mathcal{D}, \{x_j^{(k)}\}_{j=1}^D, \{x_j^{(k)}\}_{k=1}^M)$   
10: Train RF to discriminate real vs generated samples and compute  $\text{RF}_{\text{acc}}$   
11: **return**  $\{\text{stat}_j\}$ , MMD,  $\text{RF}_{\text{acc}}$

---



---

#### Algorithm 4 Interventional Sampling

---

**Require:** Dataset  $\mathcal{D}$  in causal order, functions  $f_\theta$ , intervention values  $\{\alpha_j\}_{j \in \mathcal{I}}, M$   
**Ensure:**  $\{x_j^{(k)}\}_{j=1}^D, \{x_j^{(k)}\}_{k=1}^M$   
1: **for**  $j \in \mathcal{I}$  **do**  
2:    $x_j \leftarrow \alpha_j$   
3: **end for**  
4: **for**  $j \in \{1, \dots, D\} \setminus \mathcal{I}$  **do**  
5:   Sample  $\{u_j^{(k)}\}_{k=1}^M \sim \tilde{p}(u_j)$   
6:    $x_j^{(k)} \leftarrow \tilde{f}(\text{pa}(j)^{(k)}) + u_j^{(k)}$   
7: **end for**  
8: **return** generated interventional samples

---

### C. Hyperparameter search

The experiments were conducted after a hyperparameter search. We include here the specific grid that we used to increase reproducibility.

**Algorithm 5** Counterfactual Inference**Require:** Factual covariates  $\mathbf{x}^f$  in causal order, functions  $f_\theta$ , intervention set  $\mathcal{I}$ **Ensure:** Counterfactual covariates  $\{x_j\}_{j=1}^D$ 

```

1: for  $j = D$  down to 1 do
2:    $\tilde{u}_j^f \leftarrow x_j^f - f_\theta(\text{pa}(j)^f)$ 
3: end for
4: for  $j \in \mathcal{I}$  do
5:    $x_j \leftarrow \alpha_j$ 
6: end for
7: for  $j \in \{1, \dots, D\} \setminus \mathcal{I}$  do
8:    $x_j \leftarrow f_\theta(\text{pa}(j)^{\text{cf}}) + \tilde{u}_j^f$ 
9: end for
10: return  $\{x_j\}_{j=1}^D$ 

```

- KAN: Hidden dimension size (0, 5); Grid size (1, 5, 10); Learning rate ( $1e-3, 1e-3, 1e-4$ ), L1 regressor strength (0.1, 0.01, 0.001), Use of multiplicative nodes (yes or no, binary option).
- DBCM: Number of training epochs (100, 200, 500); Learning rate ( $1e-2, 1e-3, 1e-4$ ); Batch size (32, 64, 128), Hidden dimension size (32, 64, 128).
- CFlow: Flow type (CausalNSF or CausalMAF); Hidden dimension sizes ((32, 32), (64, 64), (64, 64, 64), (128, 128)); Learning rates ( $1e-2, 1e-3, 1e-4, 1e-5$ ); Scheduler (None or plateau); Number of bins (4, 8, 16).

We then select, for each child, the best hyperparameter combination based on the RF accuracy between the generated and the observational data for the child and all covariates in the graph. In order to find the best KAAM hyperparameters, we reuse the results of the KAN grid search, and keep the best hyperparameters per child among those who had no hidden dimension (hidden dimension size is 0) and do not make use of multiplicative nodes.

For DBCM and CFlow, we select based on RF accuracy between the generated and the observational data. Finally, for ANM, the library used does an automatic search to find the best model in terms of regression performance.

*D. Benchmark graphs description*

We now introduce the 11 synthetic graphs used for benchmarking in §V of this work. The graphs are based on [29], and are designed to provide a combination of linear and non-linear equations. All exogenous variables  $u_i$  follow a standard Gaussian distribution  $\mathcal{N}(0, 1)$  and we standardize all variables before generating the next one.

**3 Chain Linear**

$$\begin{cases} x_1 = f_1(u_1) = u_1 \\ x_2 = f_2(x_1, u_2) = 10 \cdot x_1 - u_2 \\ x_3 = f_3(x_2, u_3) = 0.25 \cdot x_2 + 2 \cdot u_3 \end{cases}$$

**3 Chain non Linear**

$$\begin{cases} x_1 = f_1(u_1) = u_1 \\ x_2 = f_2(x_1, u_2) = e^{0.5 \cdot x_1} + 0.25 \cdot u_2 \\ x_3 = f_3(x_2, u_3) = \frac{(x_2 - 5)^3}{15} + u_3 \end{cases}$$

**4 Chain Linear**

$$\begin{cases} x_1 = f_1(u_1) = u_1 \\ x_2 = f_2(x_1, u_2) = 5 \cdot x_1 - u_2 \\ x_3 = f_3(x_2, u_3) = -0.5 \cdot x_2 - 1.5 \cdot u_3 \\ x_4 = f_4(x_3, u_4) = x_3 + u_4 \end{cases}$$

**5 Chain Linear**

$$\begin{cases} x_1 = f_1(u_1) = u_1 \\ x_2 = f_2(x_1, u_2) = 10 \cdot x_1 - u_2 \\ x_3 = f_3(x_2, u_3) = 0.25 \cdot x_2 + 2 \cdot u_3 \\ x_4 = f_4(x_3, u_4) = x_3 + u_4 \\ x_5 = f_5(x_4, u_5) = -x_4 + u_5 \end{cases}$$

**Collider Linear**

$$\begin{cases} x_1 = f_1(u_1) = u_1 \\ x_2 = f_2(u_2) = 2 - u_2 \\ x_3 = f_3(x_1, x_2, u_3) = 0.25 \cdot x_2 - 0.5 \cdot x_1 + 0.5 \cdot u_3 \end{cases}$$

**Fork Linear**

$$\begin{cases} x_1 = f_1(u_1) = u_1 \\ x_2 = f_2(u_2) = 2 - u_2 \\ x_3 = f_3(x_1, x_2, u_3) = 0.25 \cdot x_2 - 1.5 \cdot x_1 + 0.5 \cdot u_3 \\ x_4 = f_4(x_3, u_4) = x_3 + 0.25 \cdot u_4 \end{cases}$$

**Fork non Linear**

$$\begin{cases} x_1 = f_1(u_1) = u_1 \\ x_2 = f_2(u_2) = u_2 \\ x_3 = f_3(x_1, x_2, u_3) = \frac{4}{1 + e^{-x_1 - x_2}} - x_2^2 + 0.5 \cdot u_3 \\ x_4 = f_4(x_3, u_4) = \frac{20}{1 + e^{0.5 \cdot x_3^2 - x_3}} + u_4 \end{cases}$$

**Simpson non Linear**

$$\begin{cases} x_1 = f_1(u_1) = u_1 \\ x_2 = f_2(x_1, u_2) = \log(1 + e^{1 - x_1}) + \sqrt{\frac{3}{20}} u_2 \\ x_3 = f_3(x_1, x_2, u_3) = \tanh(2 \cdot x_2) + 1.5 \cdot x_1 - 1 + \tanh(u_3) \\ x_4 = f_4(x_3, u_4) = \frac{x_3 - 4}{5} + 3 + \frac{u_4}{\sqrt{10}} \end{cases}$$

**Simpson Symprod**

$$\begin{cases} x_1 = f_1(u_1) = u_1 \\ x_2 = f_2(x_1, u_2) = 2 \cdot \tanh(2 \cdot x_1) + \frac{u_2}{\sqrt{10}} \\ x_3 = f_3(x_1, x_2, u_3) = 0.5 \cdot x_1 \cdot x_2 + \frac{u_3}{\sqrt{2}} \\ x_4 = f_4(x_1, u_4) = \tanh(1.5 \cdot x_1) + \sqrt{\frac{3}{10}} \cdot u_4 \end{cases}$$

**Triangle Linear**

$$\begin{cases} x_1 = f_1(u_1) = u_1 \\ x_2 = f_2(x_1, u_2) = 10 \cdot x_1 - u_2 \\ x_3 = f_3(x_1, x_2, u_3) = 0.5 \cdot x_2 + x_1 + u_3 \end{cases}$$

**Triangle non Linear**

$$\begin{cases} x_1 = f_1(u_1) = u_1 \\ x_2 = f_2(x_1, u_2) = 2 \cdot x_1^2 + u_2 \\ x_3 = f_3(x_1, x_2, u_3) = \frac{20}{1+e^{-x_2^2+x_1}} + u_3 \end{cases}$$

Note that all of the above graphs are continuous. In order to obtain their mixed counterparts, we chose to always discretize  $x_3$  by using the following procedure:

- First, we standardize  $x_3$ .
- Then, we sample a discrete ternary variable, with values  $\{0, 1, 2\}$ , with the following probability vector:
  - If  $x_3 < -1$ , the probability vector is  $[0.8, 0.1, 0.1]$ .
  - If  $x_3 > 1$ , the probability vector is  $[0.1, 0.1, 0.8]$ .
  - In any other case, the probability vector is  $[0.1, 0.8, 0.1]$ .

Note that the procedure is not deterministic because we sample a categorical random variable, hence, we introduce additional noise when discretizing the covariate.

### E. Training times

Here we report training times for completeness, in Tab III.

	Continuous	Discrete	Sachs Additive	Sachs Nonadditive
KAN	17.71 <sub>20.5</sub>	37.88 <sub>52.5</sub>	374.90 <sub>53.51</sub>	385.17 <sub>66.42</sub>
KAAM	13.79 <sub>5.6</sub>	3.36 <sub>2.98</sub>	356.39 <sub>20.92</sub>	345.11 <sub>49.96</sub>
ANM	0.02 <sub>0.0</sub>	0.02 <sub>0.02</sub>	0.28 <sub>0.25</sub>	0.20 <sub>0.21</sub>
DBCM	11.19 <sub>8.3</sub>	6.74 <sub>6.28</sub>	502.45 <sub>120.63</sub>	483.95 <sub>134.50</sub>
CFlow	3.12 <sub>2.8</sub>	2.92 <sub>2.20</sub>	1.49 <sub>0.51</sub>	9.33 <sub>9.12</sub>
KAN <sub>mix</sub>	—	7.45 <sub>33.93</sub>	—	—
KAAM <sub>mix</sub>	—	10.93 <sub>7.96</sub>	—	—

Table III: Training time in seconds across experiments, reported as averages over datasets or runs ( $\text{mean}_{\text{std}}$ ). Continuous and discrete correspond to the synthetic experiments.

### F. Biographies



**ALEJANDRO ALMODOVAR** received the B.S. degree and the M.Sc. degree in communications engineering from Universidad Politécnica de Madrid (UPM), Madrid, Spain, in 2020 and 2022, respectively. Currently, he is a Ph.D. student whose work focuses on causal inference with deep learning, with applications in medicine and healthcare, among others.



**MAR ELIZO** received the B.S. degree in Computer Engineering from the Universidad Carlos III de Madrid (UC3M) in 2023, and the M.Sc. degree in Artificial Intelligence, Pattern Recognition, and Digital Imaging from the Universitat Politècnica de València (UPV) in 2024. She is currently pursuing a Ph.D. degree at Universidad Politécnica de Madrid (UPM), focusing on deep learning and causal inference applications in healthcare.



**PATRICIA A. APELLÁNIZ** received the B.S. degree in Telecommunication Engineering from the Universidad Autónoma de Madrid, Spain, in 2018, and the M.Sc. and Ph.D degrees in Telecommunication Engineering from the Universidad Politécnica de Madrid (UPM), Spain (2020 and 2025, respectively). She is currently a researcher and teaching collaborator at UPM. Her research interests include deep learning for healthcare and signal processing.



**JUAN PARRAS** received the B.S. degree in telecommunications engineering from the Universidad de Jaén in 2014, and the M.Sc. and Ph.D. degrees in telecommunications engineering from the Universidad Politécnica de Madrid (UPM) in 2016 and 2020, respectively. He is currently an Assistant Professor with UPM. His research interests include deep generative models, deep reinforcement learning, game theory, and optimization with health and communications applications.



**SANTIAGO ZAZO** is currently a Dr. Engineer with the Universidad Politécnica de Madrid (UPM), since 1995. In 1998, he joined UPM, where he is currently a Full Professor in signal theory and communications. More recently, he has been mostly focused on deep learning with medical applications, distributed optimization, game theory, and reinforcement learning. He is the author/co-author of more than 40 journal articles and about 200 conference papers. His main research interest includes signal processing.